Effects of Pressure on Maghemite Nanoparticles With a Core/Shell Structure

Y. Komorida[1,*] , M. Mito[1] , H. Deguchi[1], S. Takagi[1], T. Tajiri[2],

A. Millán[3], N. J. O. Silva[3], M. A. Laguna[3] and F. Palacio[3]

[1]*Faculty of Engineering, Kyushu Institute of Technology, Kitakyushu, 804-8550, Japan*

[2]*Faculty of Science, Fukuoka University, Fukuoka, 814-0180, Japan*

[3]*Instituto de Ciencia de Materiales de Aragón, CSIC-Universidad de Zaragoza, Zaragoza,*

50009, Spain

\<Abstract\>

The magnetic property and intra-particle structure of the γ phase of Fe_2O_3 (maghemite) nanoparticles with a diameter (D) of 5.1 $\pm$ 0.5 nm were investigated through AC and DC magnetic measurements and powder X-ray diffraction (XRD) measurements at pressures (P) up to 27.7 kbar. Maghemite originally exhibits ferrimagnetic ordering at about 918 K, and has an inverse spinel structure with vacancies. Maghemite nanoparticles studied here consist of a superparamagnetic core with structural periodicity and a disordered shell without the periodicity. The DC and AC susceptibilities reveal that the anisotropy energy barrier ($\Delta E/k_B$) decreases at the initial pressure ($P \leq 3.8$ kbar), recovering at $P \geq 3.8$ kbar. The physical mechanism associated to the change of $\Delta E/k_B$ with P suggests that it is associated to the existence of a down-and-up fluctuation of the number of Fe^{3+} ions constituting the core at the pressure threshold of about 4 kbar. This phenomenon was confirmed by the analysis of the

1

XRD measurement using Scherrer's formula. The core volume decreased down to about 45 % of the initial volume at $P = 2.5$ kbar. The result series obtained in this study indicates that both the core and the shell are unstable against external stress, and that, at higher pressure, the core can be restructured. $\Delta E/k_B$ is approximately proportional to the volume associated to the ordered fraction of the nanoparticles as seen from XRD, V_{core}. From this dependence it is possible to separate the core/shell contribution to $\Delta E/k_B$ and estimate a core and surface anisotropy constants, with the core one being of the order of magnetocrystaline anisotropy of maghemite. As for the structural experiments, the data for $D = 12.8 \pm 3.2$ nm at pressures of up to $P = 33.6$ kbar are also presented.

KEYWORDS: pressure effects, nanoparticle, core/shell structure, maghemite, superparamagnetism

PACS: 75.50.Tt, 75.75.+a, 61.46.Df, 81.40.Vw

[*]corresponding author
Yuki Komorida
1-1 Sensui-cho, Tobata-ku, Kitakyushu, 804-8550, JAPAN
tel&fax. ;81-93-884-3286
e-mail: g586402y@tobata.isc.kyutech.ac.jp

1. Introduction

Nowadays, the magnetic study of nanoparticles is one of the most active research areas of condensed matter physics from the viewpoints of both fundamental science and industrial application. When the particle size reaches the nano-meter scale, superparamagnetism appears due to single-domain formation [1, 2]. The magnetically active state of this minuscule domain leads us to believe that it is possible to apply it to high-bit information storage devices. Physically, the effect of surface is quite interesting. The structural defects in the surface can bring about complex magnetic behavior, and the influence of the defects is more remarkable than in bulk systems. On the other hand, inter-particle interaction via the spins of the surface also affects the magnetic properties [3]. A fundamental understanding of the basic physical properties of magnetic nanoparticles is an important stimulant to the development of nano-science and advanced technologies.

Iron oxide nanoparticles have already been also used in several biomedical fields like magnetic resonance imaging, hyperthermia targeted drug delivery and tissue engineering [4]. Among iron oxides, the γ phase of Fe_2O_3 (maghemite) is one of the most attractive materials for industrial application because of its chemical stability. Maghemite originally exhibits ferrimagnetic ordering below about 918 K [5]. The basic structure of bulk maghemite is the inverse-spinel structure with some vacant sites, and possesses cubic symmetry ($P4_332$) with a lattice constant of $a = 8.34$ Å [6, 7]. However, the recent structural study has revealed that the ordered distribution of the caution vacancies on the octahedral positions results in the formation of the tetragonal superlattice (space group $P4_12_12$) [6, 7]. In the case of maghemite, the existence of these vacancies strongly influences the generation of the net moment. Especially in nanoparticles with many surface molecules, the effect becomes considerable, and in fact the magnetic properties are dependent on the synthesis method [8, 9].

Here, let us briefly describe the core/shell structure of ferrimagnetic nanoparticles. The

expression "core/shell structure" provides an important clue to the magnetic properties of *ferrimagnetic* nanoparticles. The central part, *i.e.*, the core, has structural periodicity, and can maintain spontaneous magnetization, which results in superparamagnetism. In contrast, the surface region, *i.e.*, the shell, has no structural periodicity. There is no evidence of an abrupt change between the core with structural periodicity and the disordered shell and in practice there must be a more or less extended transition between core and shell. In this view, the core-shell model is an approximation that, however, has been successfully used to model the magnetic properties of nanoparticles [10-14]. The net moment of the entire particle originates from the moment of the core. The magnetic properties of the surface shell are often described as approaching those of disordered systems as spin glasses [15], and are analyzed as paramagnetic/antiferromagnetic component in the magnetization curve data [16]. In the frame of the core-shell model, the magnetic behavior of maghemite nanoparticle systems is understood in terms of the magnetic properties of the core and the shell. In the maghemite nanoparticles, Millán *et al.* [16] have reported an interesting result that the shell thickness is independent of the particle size, and is estimated to be about 1 nm, in particles with size ranging from 2 to 15 nm, through the analysis of magnetization curve data. The magnetic interaction between the core and the shell can appear as an exchange bias effect, among other characteristics. A fundamental study of these two components of a ferrimagnetic nanoparticle system allows us to gain insight into the physics of defects and surface effects. Thus, we deemed it necessary to investigate the magnetic properties of a prototype material by applying pressure to it and thereby changing its structural background systematically. Pressurization was expected to continuously shrink and restructure the system and tune the defects. We have already reported the preliminary results for maghemite nanoparticles with a diameter (D) of 6.5 ± 0.65 nm, and confirmed the changes in the magnetic properties under pressure [17]. In this paper, we report the effects of hydrostatic pressure on both the magnetic properties and

the intra-particle structure in maghemite nanoparticles with $D = 5.1 \pm 0.5$ nm, according to magnetic measurements and structural analyses. As for the structural analysis experiments, the experimental data for $D = 12.8 \pm 3.2$ nm are also presented, in order to show that the effects of pressure are independent of the particle size in the nano-size level.

2. Experimental

The two kinds of maghemite nanoparticles used in this study were prepared by a procedure mentioned elsewhere [16], in which the nanoparticles are grown within an organic polymeric matrix of polyvinylpyridine (PVP) that coats the particles and prevents aggregation. Transmission electron microscopy (TEM) images and size distributions are given in Fig. 1. The diameter, D, had been estimated to be $D = 5.1 \pm 0.5$ nm and $D = 12.8 \pm 3.2$ nm by means of TEM images. These samples were annealed at 200°C and 250°C, respectively. Against the total mass of these samples including PVP, the weight percentage of maghemite is estimated to be 9 wt% ($D = 5.1$ nm) and 37 wt% ($D = 12.8$ nm).

The AC and DC magnetic measurements were done using a superconducting quantum interference device (SQUID) magnetometer (Quantum Design, MPMS-5S) in the temperature (T) range of 5 K $\leq T \leq$ 80 K. Pressure was attained using a piston cylinder cell (CR-PSC-KY05-1, Kyowa-Seisakusho Co., Ltd.), which can be inserted into the SQUID magnetometer [18]. The pressure cell was made of a non-magnetic Cu-Be alloy. In order to apply pressure effectively, the sample was held inside the teflon cell with the aid of a pressure-transmitting medium, Apiezon-J oil, and a small amount of metallic superconductor tin. The pressures at liquid-helium temperature were estimated based on the shift in the superconducting transition temperature of the tin [19].

Synchrotron radiation powder X-ray diffraction (XRD) measurements were performed at pressures up to 33.6 kbar using a cylindrical imaging plate (IP) diffractometer (Rigaku Co.) at the Photon Factory (PF) of the Institute of Materials Structure Science, the High Energy

Accelerator Research Organization (KEK) [20]. The powder XRD pattern was measured at room temperature. The wavelength of the incident X-ray λ was 0.6883(1) Å. Pressurization was performed by the use of a diamond anvil cell (DAC) with a Be backing plate, on which diamond anvils with 0.8-mm flat tips were mounted. Between the anvils, a 0.3-mm thick Cu-Be gasket was inserted. In the sample hole with a diameter of 0.4 mm located in the center of the gasket, the crystalline sample and a few ruby crystals were held with the aid of a pressure-transmitting medium, fluorine oil (FC77). The pressure value was calibrated by the ruby fluorescence method [21], and the estimated value of pressure involves the measurement error of ± 0.8 kbar.

3. Experimental Results

3.1. Magnetic properties

  The magnetic properties of maghemite nanoparticles with $D = 5.1$ nm were investigated through the following three magnetic measurements: AC susceptibility measurement, and zero-field-cooled (ZFC) and field-cooled (FC, from $T = 80$ K and $H = 200$ Oe) DC magnetization measurements. In the AC measurement, the frequency range of the AC exciting field was 1-100 Hz, and the field amplitude was 2.0 Oe.

DC magnetic susceptibility

  Figure 2 shows the temperature dependence of the ZFC and FC magnetization (M) under pressure for maghemite nanoparticles with $D = 5.1$ nm. The arrows indicate the peak positions of ZFC magnetization (T_p). The value of T_p at ambient pressure was estimated to be 12.3 ± 0.5 K. When a pressure of 3.8 kbar was applied, the T_p decreased to 11.2 ± 0.5 K. However, further pressurization unexpectedly increased the T_p, following an unexpected down-and-up

fluctuation of pattern.

Figure 3 shows the temperature dependence of the deviation between the FC and ZFC magnetizations, $\Delta M_{\text{FC-ZFC}}(T)$, at several pressures. The data for $\Delta M_{\text{FC-ZFC}}(T)$ gives us the information on the temperature region of thermal irreversibility. The $\Delta M_{\text{FC-ZFC}}$ at ambient pressure rapidly increased with decreasing temperature below 30 K. When a pressure of 3.8 kbar was applied, the overall behavior of $\Delta M_{\text{FC-ZFC}}(T)$ curve shifted toward the lower-temperature side. Thereafter, upon further pressurization, it shifted toward the higher-temperature side. The pressure dependence of $\Delta M_{\text{FC-ZFC}}(T)$ is consistent with the change in T_{p}. The above characteristic pressure dependencies (the down-and-up fluctuation of T_{p} and $M_{\text{FC-ZFC}}(T)$) have already been observed in maghemite nanoparticles with $D = 6.5$ nm [17].

AC magnetic susceptibility

Figure 4 shows the temperature dependence of the out-of-phase component of the AC magnetic susceptibility, χ'', at $f = 1$ Hz (a) and 10 Hz (b). The out-of-phase component is related to energy loss, and the peak position allows us to determine the temperature of magnetic freezing, the so-called "blocking temperature" (T_{B}). The insets of Figure 4 show the temperature dependence of the data around T_{B}. The arrows represent the positions of T_{B} under each pressure. The pressure dependencies of T_{B} at $f = 1$ Hz and 10 Hz are plotted in Figure 5 showing a good consistency with the results for T_{p} and $\Delta M_{\text{FC-ZFC}}(T)$ mentioned above.

The frequency dependence of T_{B} at each pressure was analyzed using the Arrhénius plot, *i.e.*, the plots of the inverse of the blocking temperature, $1/T_{\text{B}}$, versus the natural logarithm of the AC frequency, $\ln(2\pi f)$. Here, the effective energy barrier, ΔE, between the spin-up and spin-down states can be estimated using the following equation:

$$\frac{1}{T_{\mathrm{B}}} = -\frac{k_{\mathrm{B}}}{\Delta E}\left\{\ln(2\pi f) + \ln(\tau_0)\right\},\tag{1}$$

where k_{B} is the Boltzmann constant, and τ_0 is a pre-exponential factor. The Arrhénius plots for the present experiment are shown in Figure 6. The solid lines show the fitting data using Eq. (1), and ΔE was estimated from the slope. The inset of Figure 6 shows the pressure dependence of $\Delta E/k_{\mathrm{B}}$, which is also qualitatively consistent with the results series for T_{p}, $\Delta M_{\mathrm{FC\text{-}ZFC}}$ and T_{B}. At ambient pressure, the value of $\Delta E/k_{\mathrm{B}}$ was estimated to be 378 K. At P = 3.8 kbar, the value of $\Delta E/k_{\mathrm{B}}$ decreased to 88.7 % of the initial value. At P = 14.3 kbar, it increased to 111 % of the initial value. Thus, quantitative analyses on the T_{B} and $\Delta E/k_{\mathrm{B}}$ reveal that the average energy barrier ΔE is reduced and thereafter enhanced. Disregarding interparticle interactions, the decreases of the onset of thermal irreversibility (seen in $\Delta M_{\mathrm{FC\text{-}ZFC}}$) and of T_{B} are associated to a decrease of the energy barrier of the particles with larger anisotropy energy. In this view, both the particles with average ΔE and the particles with higher ΔE follow the same down-and-up trend. Together, these experimental features show the existence of a characteristic pressure P_{C} (~4 kbar), and point out the possibility that the spatial region of the core is temporarily shrunk at $P < P_{\mathrm{C}}$, whereas at $P > P_{\mathrm{C}}$, the core region is re-stabilized due to restructuring resulting from a large external stress. This suggests that the nanoparticle structure is quite sensitive to external stress, and does not have sufficient stability (elasticity) even under small stress. In order to have a better insight on the role played by the structural changes we performed the XRD experiments under pressure at room temperature.

3.2. X-ray diffraction (XRD) measurements

Synchrotron radiation powder X-ray diffraction (XRD) measurements of maghemite nanoparticles with $D = 5.1$ nm were performed at room temperature at pressures of up to 27.7 kbar. So as to prove the validity of the obtained pressure response for $D = 5.1$ nm, the data for $D = 12.8$ nm are also presented.

Figure 7 shows the XRD patterns of maghemite nanoparticles with $D = 5.1$ nm and 12.8 nm. These diffraction patterns are consistent with the Rietveld simulation based on the space group $P4_332$ with $a = 8.34$ Å (labeled with (a)), whereas the intensities of these patterns were not perfectly reproduced by the simulation especially around $2\theta = 16°$, owing to the effects of the nano-scale size. In such a case, the Rietveld analysis cannot be an effective analytic approach, even if the effective backgrounds (b) and (c) are assumed. In particular, for $D = 5.1$ nm, at around $2\theta = 16°$ and $27°$, the broadening owing to the nano-scale size is remarkable. Thus, the following two kinds of analytic methods were adopted. First, the lattice constant was determined from the information of the diffraction angles of some diffraction peaks. Next, the particle size of the core having structural periodicity was calculated using Scherrer's formula (Eq. 2) for the main diffraction peak of the plane index (311) around $2\theta = 16°$.

Figure 8 shows the XRD patterns for $P = 0$ (a), 2.5 (b), 8.5 (c) and 14.8 kbar (d) as representative data for maghemite nanoparticles with $D = 5.1$ nm. In the experimental data shown in Fig. 8, the contribution of the background, including the diamond anvils and FC77 (see Fig. 7), was subtracted. At first, the data for $2\theta = 12\text{-}18°$ at $P = 0$ kbar (a) could be reproduced by the summation of seven diffraction peaks with Lorentzian shape, based on $P4_332$. It reveals that vacancy sites are not ordered in the present magnetic nanoparticles. Hereafter we do the structural analyses based on $P4_332$. In particular, the diffraction peak around $2\theta = 16°$ were well fitted with the summation of three Lorentzians due to the plane indices (310), (311) and (222) even at the pressurized states. Both the full-width at

9

half-maximum (FWHM) of the diffraction peak and the diffraction peak angle for (311) were available for the following analyses.

Using the information on the dominant diffraction peak (311), the lattice constant (a) of the cubic lattice and the particle size of the core, D_{core}, were estimated. The D_{core} was calculated from the values of the FWHM and the diffraction peak angle using the Scherrer's formula, as follows:

$$D_{core} = \frac{0.9\lambda}{\beta \cos\theta},$$ (2)

where β is the FWHM of the diffraction peak expressed in radians, θ is the diffraction peak angle, and D_{core} is the particle diameter.

At ambient pressure, D_{core} was estimated to be 3.8 nm. In the present study, the thickness of the shell was calculated to be about 0.65 nm (= (D - D_{core}) / 2), at $D = 5.1$ nm and $D_{core} = 3.8$ nm. Here we consider the reason of that $D_{core} = 3.8$ nm from the XRD measurement is larger than $D_{core} = 3.1$ nm estimated according to Millán's interpretation (the thickness of the shell is about 1 nm) from the magnetic measurement [16]. The above two estimated values are derived from independent physical measurements, and do not have to be completely consistent. However, we propose the following positive reason: The entire core with the structural periodicity does not have the perfect magnetic order, and the magnetic state of the outside part of the core might be magnetically unstable. Hence, D_{core} from magnetic measurement may be smaller than that from the XRD measurement.

Figure 9 shows the pressure dependencies of the diameter of the core, D_{core} and the lattice constant (a) of the cubic lattice, estimated according to the above-mentioned procedure. The D_{core} estimated from XRD measurement reached a minimum at around 2.5 kbar, and the qualitative behavior was consistent with those of the magnetic data such as $M_{FC-ZFC}(T)$, T_p, T_B, ΔE.

As for the lattice constant of the cubic lattice, the lattice shrinkage had saturation tendency in the pressure region of 4-10 kbar. At pressures above 10 kbar, the lattice shrinkage restarted. This successive shrinkage for $P > 10$ kbar has us expect the occurrence of a structural change due to the electric repulsion between Fe^{3+} ions accompanying the restructuring of the particle. However, after the 27.7 kbar pressure was released, the diffraction pattern almost recovered to that of the initial state, and, within the considered pressure region, the elasticity of maghemite nanoparticle remained intact.

Figure 10 shows the pressure dependencies of the volume of the entire nanoparticle and that of the core. In the shell region, the unit cell cannot be defined, because the shell region does not have the structural periodicity. Here, we suppose that the shrinkage ratio of the shell is sure to equal to that of the core under pressure, since the intrinsic composition should be uniform over the entire particle. Under pressure, the particle volume, $V_{particle}$, was calculated based on the following assumption: the initial particle diameter, D, is 5.1 nm, and the shrinkage ratio of the entire nanoparticle is the same as that of the unit cell in the core under pressure. The core volume V_{core} was calculated using the diameter of the core, D_{core}, which was estimated from the analysis using the FWHM of the diffraction peak and the diffraction peak angle. The residual volume after subtracting the core volume from the particle volume at each pressure corresponded to the volume of the shell, V_{shell} ($=V_{particle} - V_{core}$).

First, let us mention the pressure dependence of $V_{particle}$, which is qualitatively similar to that of the lattice constant a, as expected. V_{core} reached a minimum at 2.5 kbar, and thereafter increased with increasing pressure. At $P = 2.5$ kbar, V_{core} was reduced to almost half of the initial volume, and the decrease ratio was much larger than that of $V_{particle}$. This suggests that the core region temporarily became quite small.

For $D = 12.8$ nm, the data corresponding to Figs. 8-10 for $D = 5.1$ nm are presented in Figs. 11-13, respectively. The essential pressure response was quite similar to that for $D = 5.1$ nm.

Figure 14 shows the ratios of V_{core}, and V_{shell}, to $V_{particle}$, under pressure for both $D = 5.1$ nm and 12.8 nm. Indeed, these ratios, $V_{core}/V_{particle}$ and $V_{shell}/V_{particle}$, are the same as the ratios of the number of Fe^{3+} ions constituting the core and shell to the number of Fe^{3+} ions constituting the entire particle. Figure 14 shows the pressure dependence of $V_{core}/V_{particle}$ and $V_{shell}/V_{particle}$ for $D = 5.1$ nm and 12.8 nm. The qualitative behavior is independent of the particle size. In particular for $D = 5.1$ nm, the number of Fe^{3+} ions constituting the core, N_{core}, was reduced to a half of the initial value at 2.5 kbar, and increased at pressures above 2.5 kbar. Finally, N_{core} at $P = 27.7$ kbar exceeded the initial value in the case of $D = 5.1$ nm. These results indicate that the core is eroded by the shell under small stress, which causes the region without structural periodicity to become enlarged. However, the larger stress saturates the particle shrinkage, and thereafter the core region is restructured and stabilized. Our series of magnetic measurement results are well explained by the change in N_{core} estimated through XRD measurements.

In the maghemite nanoparticles with $D = 25$ nm, a Raman spectroscopic study has been already done in the pressure range up to 57.5 GPa [22], and it has been reported that the γ phase transforms to the α phase at $P = 13.5$ GPa. The stability of γ-phase seen in the present experiment is consistent with the above Raman spectroscopy.

4. Discussion

In principle, changes in magnetic properties observed with the application of pressure may be attributed to interparticle and/or intraparticle effects. In the case of interparticle effects, dipolar interactions are more plausible than exchange ones, since the nanoparticles are coated with polymer. In a regular array of identical dipoles, the transition temperature associated to dipolar interactions is given by [3]

$$T_{\mathrm{d}} = \frac{a_0 \mu_0}{4\pi k_{\mathrm{B}}} \frac{m^2}{d^3} \qquad (7)$$

with a_0 being of the order of 1-10, μ_0 is the magnetic permeability of vacuum, m is the magnetic moment. d is the distance between neighboring dipoles. This expression has also been used to estimate the ordering temperature of systems of randomly distributed particles, where m and d are average values [3]. For the nanocomposite with $D = 5.1$ nm, considering $a_0 = 10$, $d = 13.8$ nm (estimated from D and from the maghemite mass concentration) and $m = 4.08 \times 10^{-18}$ emu/particle (calculated from the analysis of the magnetization curve), $T_{\mathrm{d}} = 0.5$ K at ambient pressure, which means that dipolar interactions do not play an important role in the present discussion, even considering that for the highest pressure the total volume shrinks to half. Therefore, in the present case it is quite difficult to directly detect the influence of inter-particle dipole-dipole interactions through macroscopic physical quantity measurements, magnetization measurements or AC susceptibility measurements. If the random field of the dipole-dipole interaction induces a glassy behavior, one can ascertain the sign based on the non-linear AC susceptibility. In the present study, at all pressures, no non-linear response was detected in the AC susceptibility measurement for $D = 5.1$ nm and 12.8 nm. In this view we should focus our attention on intraparticle effects.

In ferromagnetic nanoparticles, the energy barrier is expressed as proportional to volume (V) considering an effective anisotropy constant (K_{eff}) as $\Delta E = K_{\mathrm{eff}}V$. This expression is also used in ferrimagnetic nanoparticles. Surface anisotropy (K_{S}) is sometimes relevant, being expressed as an extra term in K_{eff}, such that $K_{\mathrm{eff}} = K_{\mathrm{V}} + \alpha K_{\mathrm{S}}/D$ [23]. Here, K_{V} is the volume anisotropy per unit volume. Combining information of $\Delta E/k_{\mathrm{B}}$ (P) (from Fig. 6) with information of V_{particle} (P) and V_{core} (P), we find that $\Delta E/k_{\mathrm{B}}$ is approximately proportional to V_{core} (P) (Fig. 15 (a)). From the slope of the curve, $K_{\mathrm{core}} = 7.7 \times 10^5$ erg/cm^3. This value is between that found for the magnetocrystalline anisotropy (K_1) of single-domain particle of

maghemite (K_1 = -2.5 × 10^5 erg/cm^3) [24], and that found in maghemite nanoparticles (K_1 = 3.6 - 6 × 10^6 erg/cm^3) [25]. At the same time, $\Delta E/k_B$ extrapolates to 246 ± 10 K when V_{core} = 0, corresponding to the energy barrier associated to the shell. Considering the surface of a 5.1 nm diameter nanoparticles, one can determine K_S = 4.2 × 10^{-2} erg/cm^2. This value is of the order of that previously found for maghemite nanoparticles (K_S = 6 × 10^{-2} erg/cm^2) [26], and about one order of magnitude lower than that found in Co nanoparticles (K_S = 2 - 3 × 10^{-1} erg/cm^2) [23] after analyzing K_{eff} for nanoparticles with different sizes. The above results show that the changes in $\Delta E/k_B$ induced by pressure are closely related to changes in V_{core}, with the anisotropy constant associated to $\Delta E/k_B$, the magnetic anisotropy of the core K_{core} being almost constant with P in the studied P range [27].

5. Conclusion

The effects of pressure on the γ phase of Fe_2O_3 (maghemite) nanoparticles with a diameter of 5.1 nm and 12.8 nm were studied through magnetic measurement and powder X-ray diffraction (XRD) measurement. Our experimental data series revealed that the anisotropy energy barrier $\Delta E/k_B$ decreases at the initial pressure ($P \leq 3.8$ kbar), recovering at $P \geq 3.8$ kbar. This was interpreted as a pressure-induced down-and-up fluctuation of the number of Fe^{3+} ions constituting the core. These experimental findings indicate that the core/shell structure of nanoparticles with vacancy site is unstable against external stress, and that, under high pressure, the core can be restructured.

$\Delta E/k_B$ is approximately proportional to the volume associated to the ordered fraction of the nanoparticles as seen from XRD, V_{core}. From this dependence it is possible to separate the core/shell contribution to $\Delta E/k_B$ and estimate a core and surface anisotropy constants, with the core one being of the order of magnetocrystaline anisotropy of maghemite. In this view,

14

applying pressure constitutes an elegant way of changing the core/shell ratio in an identical system in order to separate core from surface anisotropy.

Acknowledgment

References

[1] C. M. Sorensen, in: Kenneth J. Klabunde (Ed.), Nanoscale Materials in Chemistry, Wiley Interscience, New York, 2001.

[2] J. L. Dorman, D. Fiorani (Eds.), Magnetic Properties of Fine Particles, North-Holland, Amsterdam, 1992.

[3] M. F. Hansen, and S. Mørup, J. Mag. Mag. Mater. **184**, 262 (1998).

[4] D. K. Kim, Y. Zhang, W. Voit, K. V. Rao, J. Kehr, B. Bjelke, and M. Muhammed, Scripta Mater. **44**, 1713 (2001).

[5] O. Ozdemir, and S.K. Banerjee, Geophys. Res. Lett. **11**, 161 (1984).

[6] A. N. Shmakov, G. N. Kryukova, S. V. Tsybulya, A. L. Chuvilin and L. P. Solovyeva, J. Appl. Cryst. **28**, 141 (1995).

[7] Z. Somogyvári, E. Sváb, G. Mészáros, K. Krezhov, I. Nedkov, I. Sajo and F. Bourée, Appl. Phys. A **74** [Suppl.], S1077 (2002).

[8] M. P. Morales, S. Veintemillas-Verdaguer, M.I. Montero, C.J. Serna, A. Roig, Ll. Cassas, B. Martinez, and F. Sandiumenge, Chem. Mater. **11**, 3058 (1999).

[9] S. Veintemillas-Verdaguer, O. Bomati-Miguel, and M.P. Morales, Scripta Mater. **47**, 589 (2002).

[10] J. M. D. Coey, Phys. Rev. Lett. **27**, 1140 (1971).

[11] P. V. Hendriksen, F. Bødker, S. Linderoth, S. Wells, and S. Mørup, J. Phys.: Condens. Matter **6**, 3081 (1994).

[12] P. V. Hendriksen, S. Linderoth, C. A. Oxborrow, and S. Mørup, J. Phys.: Condens. Matter **6**, 3091 (1994).

[13] S. Linderoth, P. V. Hendriksen, F. Bødker, S. Wells, K. Davies, S. W. Charles, and S. Mørup, J. Appl. Phys. **75**, 6583 (1994).

[14] D. Lin, A. C. Nunes, C. F. Majkrzak, and A. E. Berkowitz, J. Mag. Mag. Mater. **145**, 343

(1995).

[15] B. Martínez, X. Obradors, Ll. Balcells, A. Rouanet, and C. Monty, Phys. Rev. Lett. **80**, 181 (1998).

[16] A. Millán, A. Urtizberea, N.J.O. Silva, F. Palacio, V.S. Amaral, E. Snoeck, and V. Serin, J. Mag. Mag. Mater. **312**, L5 (2007).

[17] Y. Komorida, M. Mito, H. Deguchi, S. Takagi, A. Millan, and F. Palacio, J. Mag. Mag. Mater. **310**, e800 (2007).

[18] M. Mito, J. Phys. Soc. Jpn. Suppl. A **76**, 182 (2007).

[19] L. D. Jennings, C. A. Swenson, Phys. Rev. **112**, 31 (1958).

[20] A. Fujiwara, K. Ishii, T. Watanuki, H. Suematsu, H. Nakao, K. Ohwada, Y. Fujii, Y. Murakami, T. Mori, H. Kawada, T. Kikegara, O. Shimomura, T. Matsubara, H. Hanabusa, S. Daicho, S. Kitamura, and C. Katayama, J. Appl. Crystallogr. **33**, 1241 (2000).

[21] G. J. Piermarini, S. Block, J. D. Barnett, and R. A. Forman, J. Appl. Phys. **46**, 2774 (1975).

[22] Z. Wang and S. K. Saxena, Solid State Commun. **123,** 195 (2002).

[23] F. Luis, J. M. Torres, L. M. García, J. Bartolomé, J. Stankiewicz, F. Petroff, F. Fettar, J. -L. Maurice, and A. Vaurès, Phys. Rev. B **65**, 094409 (2002).

[24] E. P. Valstyn, J. P. Hanton, and A. H. Morrish, Phys. Rev. **128**, 2078 (1962).

[25] B. Martínez, A. Roig, E. Molins, T. González-Carreño, and C. J. Serna, J. Appl. Phys. **83**, 3256 (1998).

[26] E. Tronc, A. Ezzir, R. Cherkaoui, C. Chanéac, M. Noguès, H. Kachkachi, D. Fiorani, A. M. Testa, J. M. Grenèche, and J. P. Jolivet, J. Mag. Mag. Mater. **221**, 63 (2000).

[27] Y. Komorida, M. Mito, H. Deguchi, S. Takagi, A. Millán, N. J. O. Silva, and F. Palacio, Appl. Phys. Lett. (in press).

Figure Legends

Figure 1.

TEM images and size distributions of maghemite nanoparticles with a diameter of 5.1 nm (a) and 12.8 nm (b).

Figure 2.

Temperature dependence of the zero-field-cooled (ZFC, open symbols) and field-cooled (FC cooling from $T = 80$ K in $H = 200$ Oe, solid lines) magnetization under various pressures for maghemite nanoparticles with $D = 5.1 \pm 0.5$ nm. The arrows indicate the peak position of the ZFC magnetization at each pressure. The base line for each piece of data for the pressure range of 3.8 – 14.3 kbar was shifted at an interval of 0.05 emu/g so as to guide the eye.

Figure 3.

Temperature dependence of the deviation between the ZFC and the FC magnetizations, ΔM_{FC-ZFC}, under several pressures for maghemite nanoparticles with $D = 5.1$ nm. The inset shows an enlargement of the rectangular area.

Figure 4.

Temperature dependence of the out-of-phase component of the AC susceptibility, χ'', at various pressures and $f = 1$ Hz (a) and 10 Hz (b) for maghemite nanoparticles with $D = 5.1$ nm.

The inset shows an enlargement of the rectangular area. The arrows indicate the blocking temperature (T_B) at each pressure. The solid curve is a visual guide.

Figure 5.

Pressure dependence of the blocking temperature (T_B) at $f = 1$ Hz and 10 Hz for maghemite nanoparticles with $D = 5.1$ nm. The solid curves are visual guides.

Figure 6.

Arrhénius plots of the inverse blocking temperature ($1/T_B$) as a function of the frequency under various pressures for maghemite nanoparticles with $D = 5.1$ nm. The solid line expresses Eq. (1) at each pressure. The inset shows the pressure dependence of the energy barrier ($\Delta E/k_B$), which is obtained from the slope of the Arrhénius plot. The solid curve is a visual guide.

Figure 7.

X-ray diffraction (XRD) patterns of maghemite nanoparticles with $D = 5.1$ nm and 12.8 nm at room temperature and ambient pressure. The open circles and squares represent the experimental data for $D = 5.1$ nm and 12.8 nm, respectively. The dotted curve (a) is the results

of a simulation based on the bulk structure. The dotted curves (b) and (c) represent the assumed background data resulting from the fluorine oil and diamond anvils for $D = 5.1$ nm and 12.8 nm, respectively.

Figure 8.

XRD patterns of maghemite nanoparticles with $D = 5.1$ nm at room temperature for $P = 0$ (a), 2.5 (b), 8.5 (c) and 14.8 kbar (d). The open squares represent the experimental data. The data for $2\theta = 12\text{-}18°$ at $P = 0$ kbar (a) could be reproduced by the summation of seven diffraction peaks with Lorentzian shape, based on $P4_332$. In particular, the diffraction peaks around $2\theta = 16°$ were fitted using the sum of three Lorentzians (red solid curve). The diffraction peaks of (310) and (222) are reproduced by the solid curves using the Lorentzians (green), while that of (311) is reproduced by the Lorentzian solid curve (blue).

Figure 9.

Pressure dependencies of the diameter of the core, D_{core}, and the lattice constant a of the cubic lattice for maghemite nanoparticles with $D = 5.1$ nm.

Figure 10.

Pressure dependencies of the volume of the entire nanoparticle, $V_{particle}$, and that of the core,

V_{core}, for maghemite nanoparticles with $D = 5.1$ nm.

Figure 11.

XRD patterns of maghemite nanoparticles with $D = 12.8$ nm at room temperature for $P = 0$ (a), 3.3 (b), 12.3 (c) and 33.6 kbar (d). The open squares represent the experimental data. The data for $2\theta = 12\text{-}18°$ at $P = 0$ kbar (a) could be reproduced by the summation of seven diffraction peaks with Lorentzian shape, based on $P4_332$. In particular, the diffraction peaks around $2\theta = 16°$ are fitted by using the sum of three Lorentzians (red solid curve). The diffraction peaks of (310) and (222) are reproduced by the solid curves using the Lorentzians (green), while that of (311) is reproduced by the Lorentzian solid curve (blue).

Figure 12.

Pressure dependencies of the diameter of the core, D_{core}, and the lattice constant a of the cubic lattice for maghemite nanoparticles with $D = 12.8$ nm.

Figure 13.

Pressure dependencies of the volume of the entire nanoparticle, $V_{particle}$, and that of the core, V_{core}, for maghemite nanoparticles with $D = 12.8$ nm.

Figure 14.

Ratios of the core volume, V_{core}, and the shell volume, V_{shell}, to the volume of the entire particle, $V_{particle}$, under pressure for $D = 5.1$ nm (a) and 12.8 nm (b). These ratios are the same as the ratios of the number of Fe^{3+} ions constituting the core and the shell to the number of Fe^{3+} ions constituting the entire particle.

Figure 15.

Anisotropy energy barrier $\Delta E/k_B$ as a function of V_{core} and $V_{particle}$ for maghemite nanoparticles with $D = 5.1$ nm. Solid line represents best linear fit to $\Delta E/k_B(V_{core})$ and dotted line its extrapolation for $V_{core} = 0$.
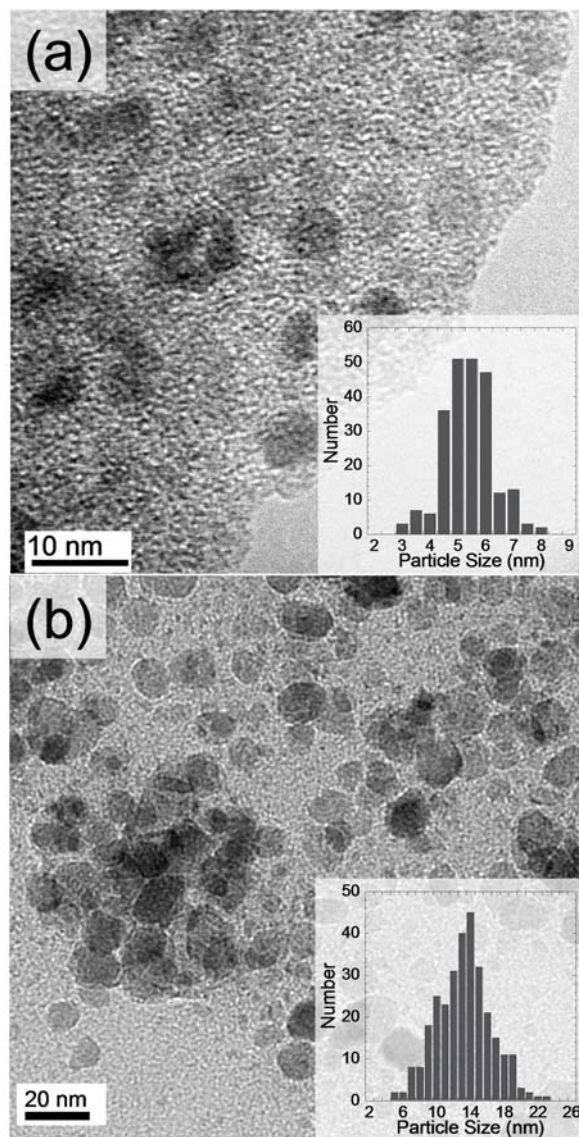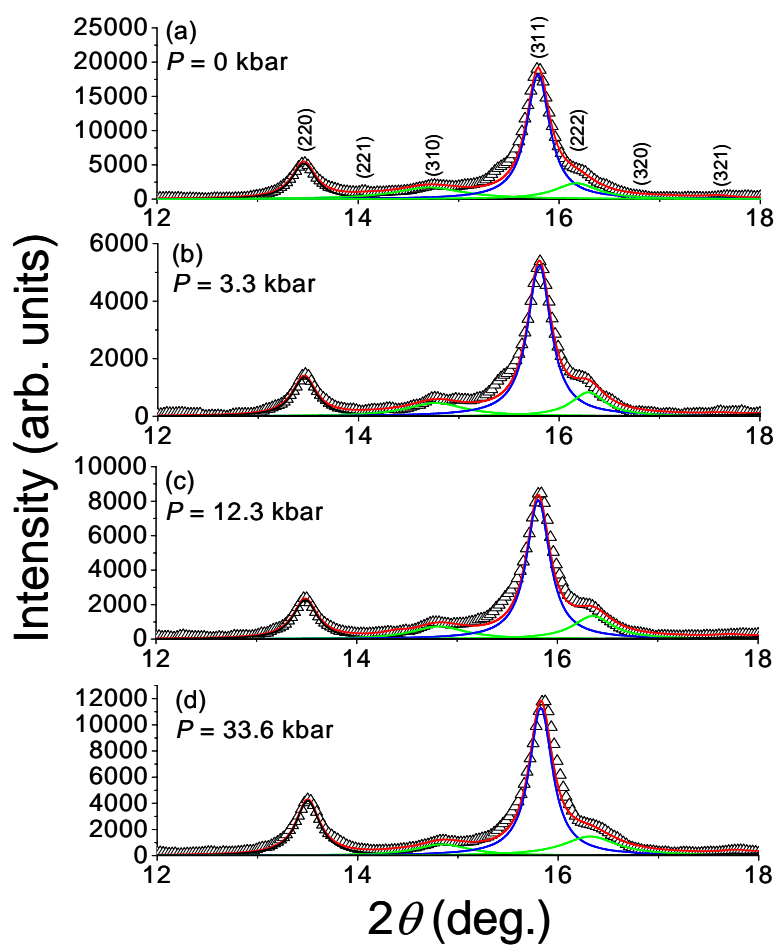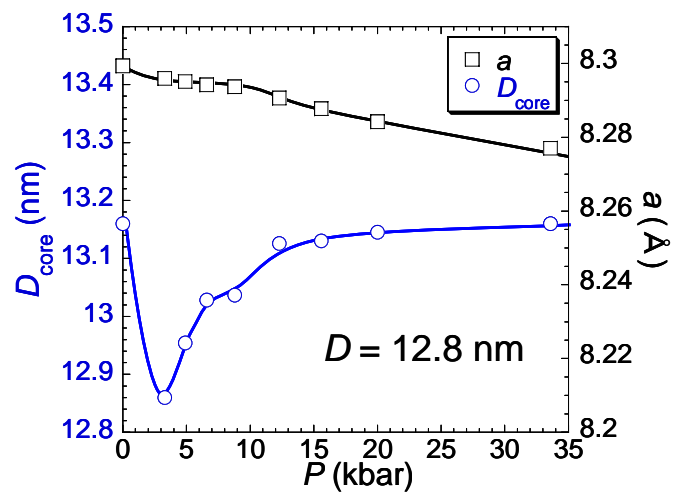
Fig. 1
Y. Komorida *et al*.
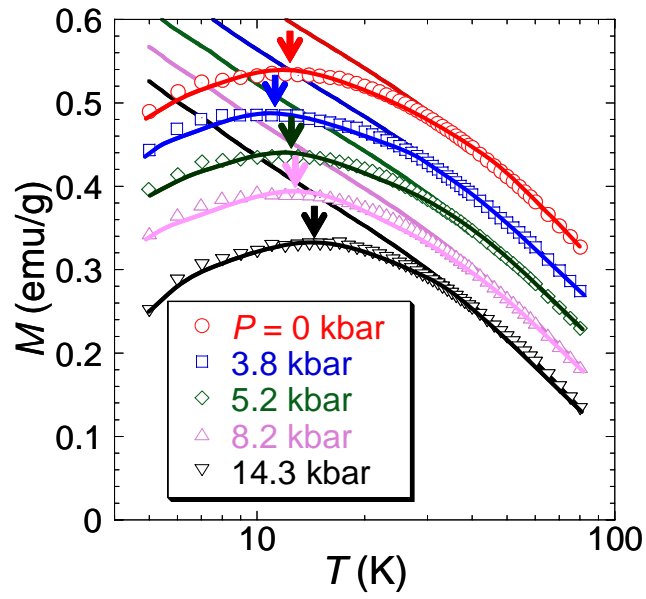
Fig. 2

Y. Komorida *et al*.
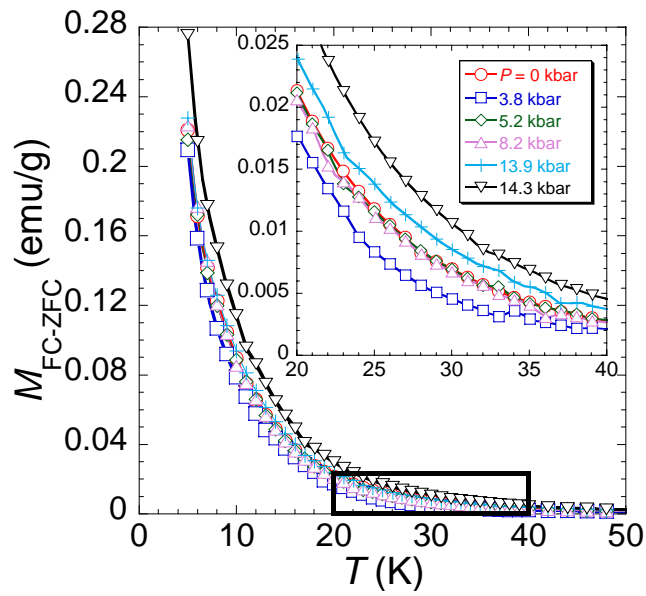
Fig. 3

Y. Komorida *et al*.
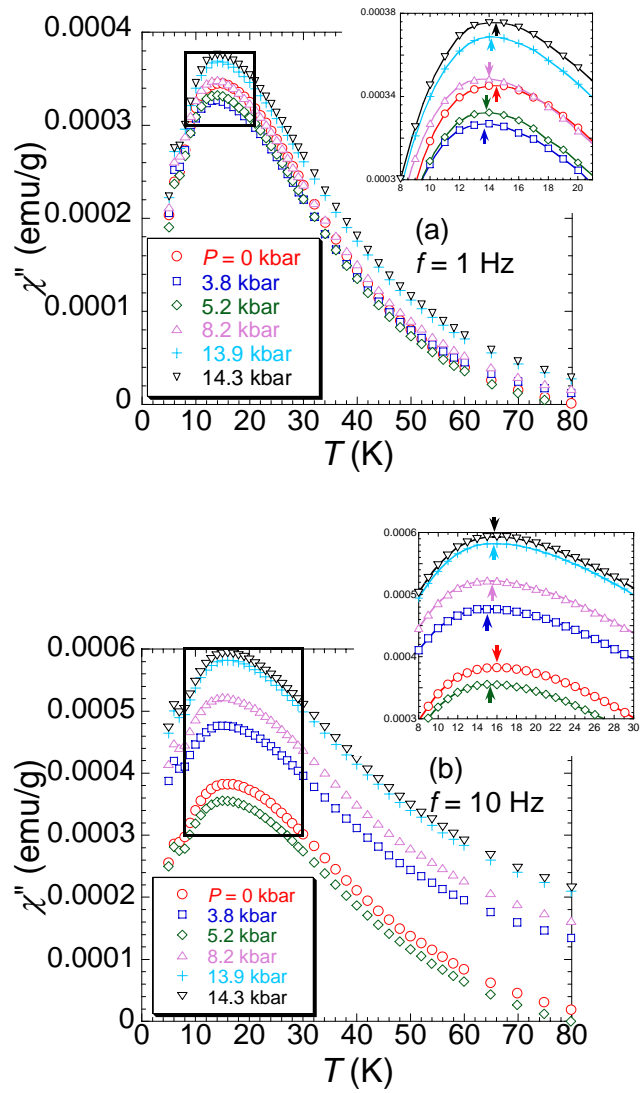
Fig. 4

Y. Komorida *et al*.
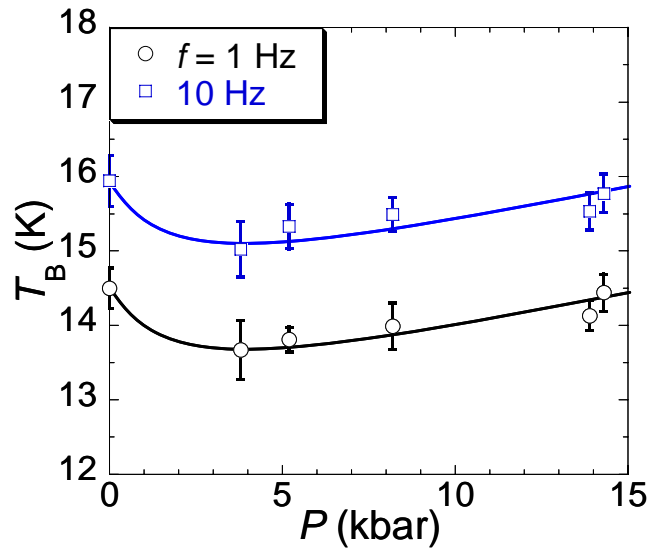
Fig. 5

Y. Komorida *et al*.
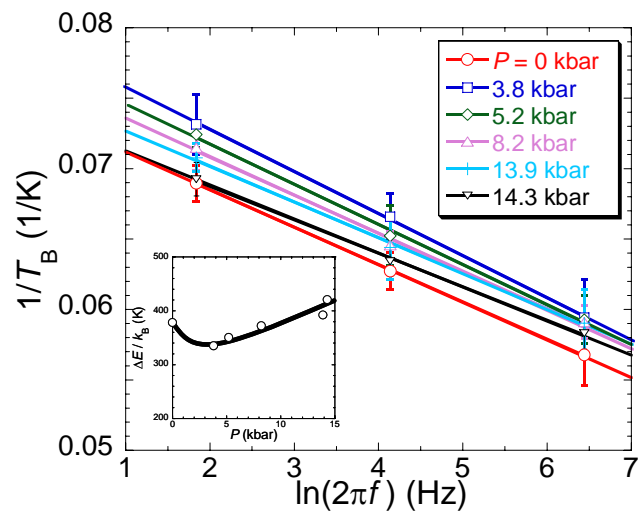
Fig. 6

Y. Komorida *et al*.
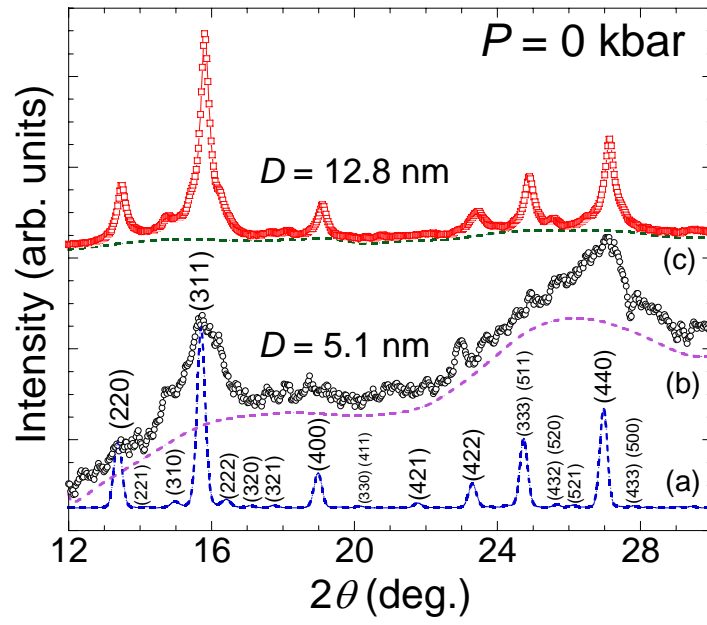
Fig. 7

Y. Komorida *et al*.
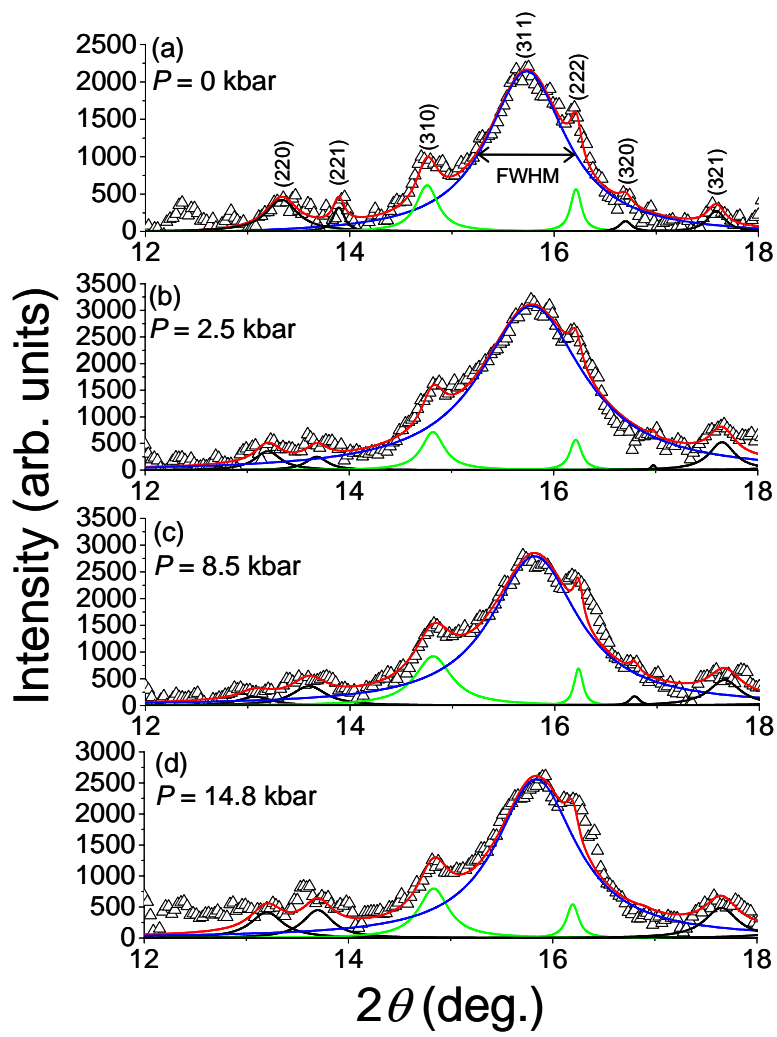
Fig. 8

Y. Komorida *et al*.
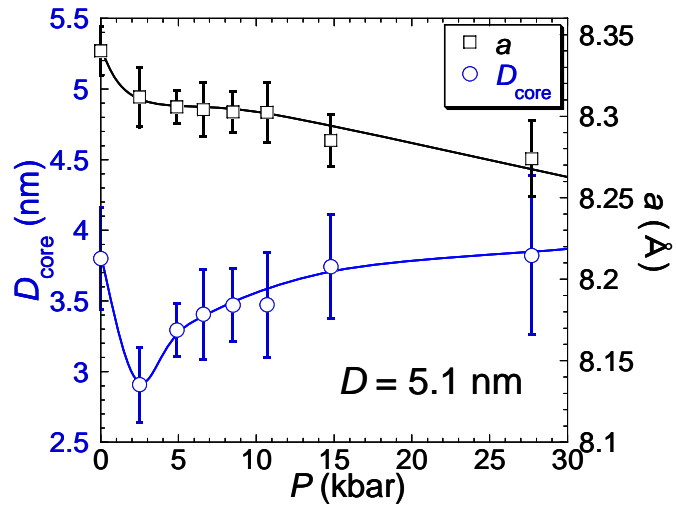
Fig. 9

Y. Komorida *et al.*
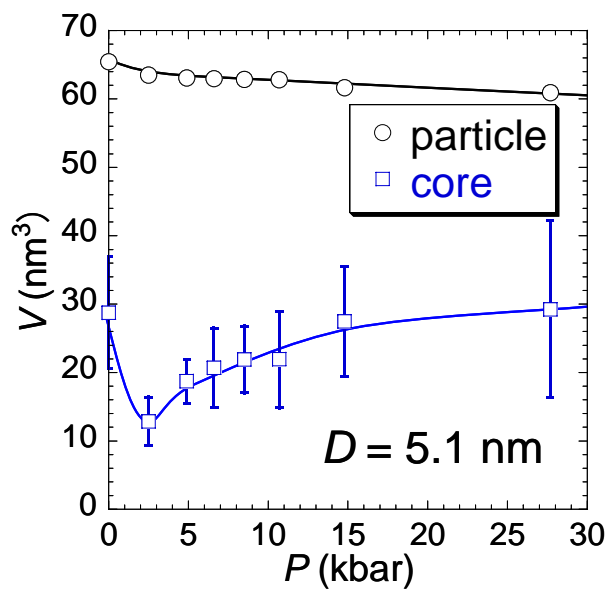
Fig. 10

Y. Komorida *et al.*

Fig. 11

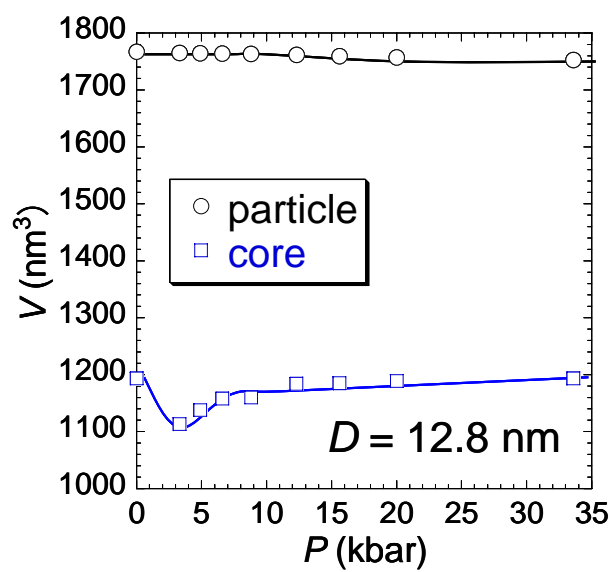Y. Komorida *et al*.

Fig. 12

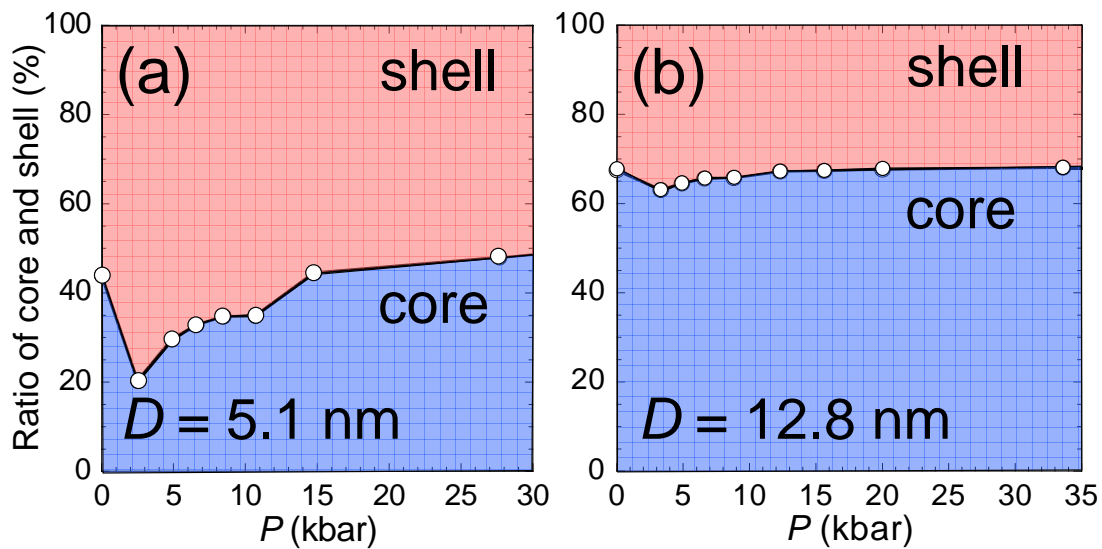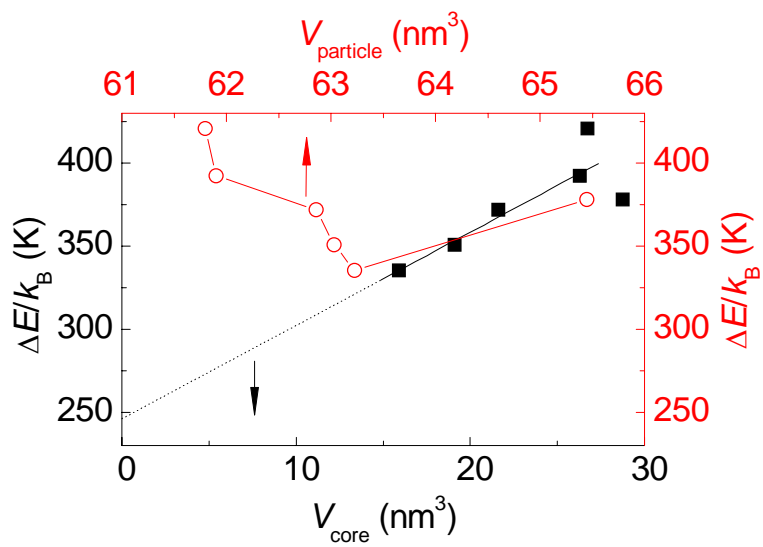Y. Komorida *et al*.

Fig. 13

Y. Komorida *et al*.

Fig. 14

Y. Komorida *et al*.

Fig. 15

Y. Komorida *et al*